PAPER

Check for updates

Instant self-healing adhesive hydrogel sensors: dual-network design for real-time human motion tracking

Yali Li,[a] Hui Liu,*[a] Ruiyao Ma,[a] Qiang Liu,[a] Shuanhong Ma, [iD] *[b] Ning Han [iD] *[c] and Ling-Bao Xing [iD] *[a]

Hydrogels are extensively utilized as strain sensors in the domain of wearable devices. However, balancing mechanical properties, adhesion, and self-healing capabilities in hydrogel sensors has consistently been a research challenge. Here, we report a facile one-pot synthesis of a double-network hydrogel integrating poly(2-(methacryloyloxy)ethyl)(dimethyl-(3-sulfopropyl)ammonium-*co*-acrylic acid) with tannic acid/polyethylenimine (as SATP), demonstrating exceptional mechanical robustness (tensile strength $\sim$0.31 MPa), high adhesion strength to diverse substrates (122.1 kPa on porcine skin), rapid self-healing (80% recovery within 1 h) and favorable conductivity (0.45 S m^{-1}), which is attributed to the dynamically reversible hydrogen bonds and electrostatic interactions. When configured as a strain sensor, the material achieves desirable sensitivity (GF = 1.27), fast response (0.84 s), and stable signal output over 500 cycles (0–300% strain). Practical applications include real-time monitoring of physiological motions from subtle facial expressions to joint movements. Notably, the hydrogel sensor can achieve information transmission through resistance modulation related to strain rate, and successfully decode the Morse code signal ("SOS") by bending the finger. This work provides a method for designing multifunctional hydrogels that simultaneously address the critical challenges of mechanical durability, environmental adaptability, and self-repair in wearable electronics, with applications in telemedicine and human-machine interfaces.
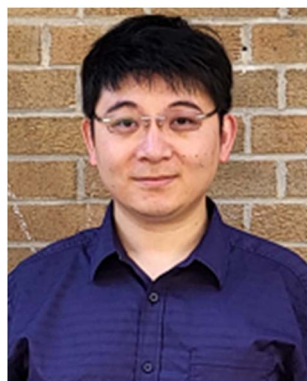
Ning Han earned his PhD from KU Leuven, Belgium, and is currently a A3MD research fellow at the University of Toronto, Canada. He has been honored with the Chinese Government Award for Outstanding Students Abroad (2021), ECS Outstanding Student Award (10 per year, 2023), Top 2% World Scientists by Stanford University (2023, 2024), and the Emerging Investigator of Royal Society of Chemistry (J. Mater. Chem. A, 2025).

Ning Han

His research focuses on applying artificial intelligence to accelerate material discovery and understanding of mechanisms, particularly for renewable fuel production.

Introduction

In recent years, flexible wearable devices have emerged as pivotal tools in health monitoring, disease diagnosis, and artificial intelligence due to their unique flexibility and extensibility, which enable conformal integration with deformable systems.[1–5] As the core component of such devices, flexible sensors must simultaneously exhibit stretchability, mechanical resilience, and biocompatibility. Conductive hydrogels, as soft, wet materials with 3D crosslinked networks, are regarded as ideal sensing materials owing to their elastic, stretchable architectures.[6–10] However, their practical applications are hindered by the need for adhesive tapes for fixation and susceptibility to damage during use, compromising stability and reusability. Thus, developing conductive hydrogels that integrate high toughness, self-adhesion, and self-healing capabilities is imperative to enhance durability and operational lifespan.

[a]School of Chemistry and Chemical Engineering, Shandong University of Technology, Zibo 255000, P. R. China. E-mail: liuhui@sdut.edu.cn; lbxing@sdut.edu.cn

[b]Shandong Laboratory of Yantai Advanced Materials and Green Manufacture, Yantai 264006, P. R. China. E-mail: mashuanhong@licp.cas.cn

[c]Department of Electrical and Computer Engineering, University of Toronto, Toronto, ON M5S 1A4, Canada. E-mail: n.han@utoronto.ca

28152 | *J. Mater. Chem. A*, 2025, 13, 28152–28159

This journal is © The Royal Society of Chemistry 2025

Recent advances have focused on improving mechanical strength, adhesion, and self-healing through chemical modifications or composite strategies. For instance, exceptional toughness is achieved *via* sacrificial bonds in double-network hydrogels,[11,12] surface adhesion is realized by dopamine modification,[13] and dynamic covalent bonds (*e.g.*, boronate esters, hydrogen bonds) enable autonomous repair.[14–16] Nevertheless, hydrogels with robust mechanical properties often exhibit strong interchain crosslinking that restricts polymer mobility, diminishing adhesion and self-healing. Conversely, highly adhesive or self-healing hydrogels typically suffer from weak mechanical strength, limiting their load-bearing applications. Resolving this trade-off to create hydrogels that simultaneously possess high toughness, ambient-condition self-repair, and adhesion remains a critical challenge.

Hydrogen bonding and electrostatic dynamic interactions are widely exploited to design tough, adhesive hydrogels due to their multivalent nature and strength, while their reversibility facilitates self-healing.[17–23] For example, Wang *et al.* replaced covalent crosslinks with tannic acid (TA)-activated dynamic interactions to develop a super-stretchable, adhesive, and self-healing hydrogel.[24] Sun *et al.* fabricated mechanically robust, self-healing polyelectrolyte films *via* layer-by-layer assembly of branched polyethyleneimine (bPEI) and poly(acrylic acid) (PAA).[25] Gong *et al.* synthesized self-healing polyampholyte (PA) hydrogels through one-pot random copolymerization of [3-(methacryloylamino)propyl]trimethylammonium chloride (MPTC) and sodium *p*-styrenesulfonate (NaSS) near the charge-balance point.[26] Notably, TA, a natural polyphenol, provides robust hydrogen bonding *via* its catechol groups, enhancing both mechanical properties and universal adhesion. As a macromolecular crosslinking agent, branched-chain PEI features abundant amine groups and minimal steric hindrance. It can enhance the toughness of materials by through electrostatic interactions and achieve self-healing through dynamic bonds.[27–29] Its cationic properties further enhance the electrostatic adhesion to biological tissues (such as skin), which has been verified in the research of biomaterials.[30]

To address these challenges, we designed a novel conductive hydrogel system, P(SBMA-AAc)/TA/PEI (as SATP), *via* a one-step synthesis using acrylic acid (AAc) and [2-(methacryloyloxy)ethyl]dimethyl-(3-sulfopropyl)ammonium (SBMA) as chemically crosslinked monomers, TA as a physical crosslinker, and PEI as a macromolecular physical crosslinker. This ternary system leverages synergistic molecular interactions: dynamic hydrogen bonds and electrostatic forces enhance interfacial adhesion, SBMA ensures stable conductivity, and PEI acts as a "bridge" to amplify crosslinking density. The resulting hydrogel exhibits remarkable mechanical properties (tensile stress: 0.31 MPa), rapid self-healing (efficiency: 80% within 1 h), and robust adhesion to diverse substrates (*e.g.*, porcine skin, adhesion strength: 122.1 kPa). The strain sensor demonstrates acceptable sensitivity (gauge factors of 0.66, 0.96, and 1.27 for 0–300% strain) while maintaining reliable detection of subtle physiological motions (*e.g.*, joint flexion, facial expressions). This work provides a versatile strategy for fabricating multifunctional hydrogel-based wearable sensors, paving the way for next-generation health-monitoring devices.
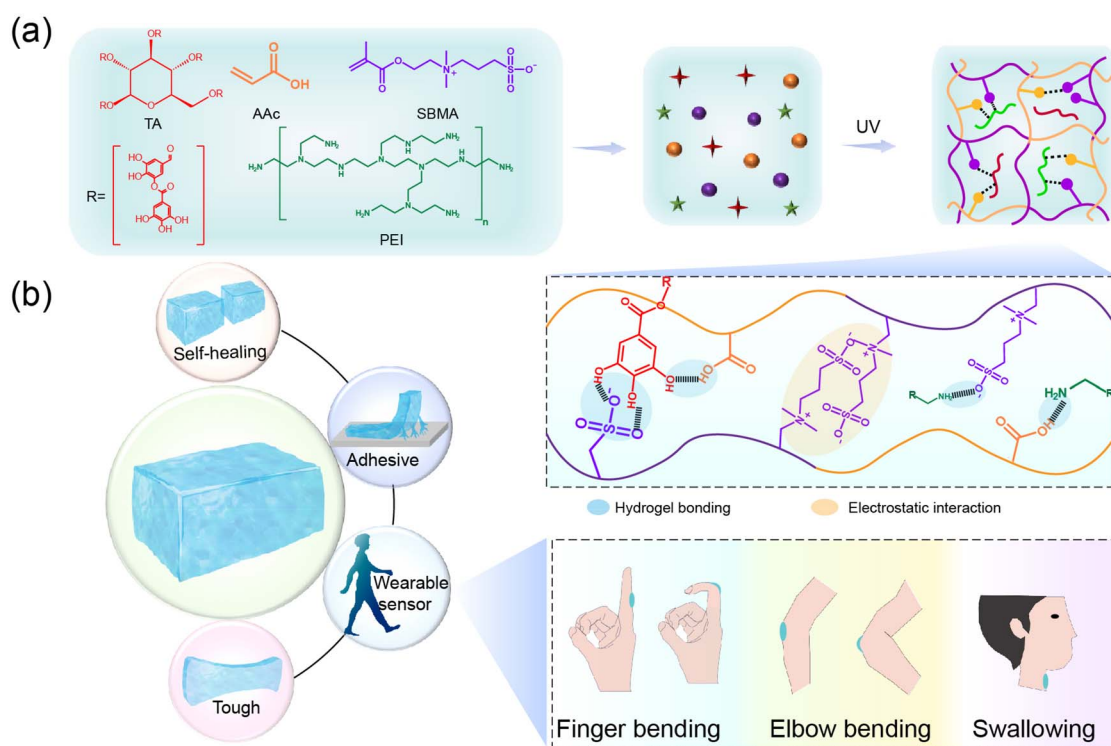

Fig. 1 (a) Schematic diagram of the synthetic process for SATP hydrogel. (b) Multiple dynamic interactions between the components and potential applications of the SATP hydrogel.

Results and discussion

Preparation of P(SBMA-AAc)/TA/PEI (as SATP) self-healing adhesive hydrogel

Herein, considering that wearable hydrogel sensor devices need to simultaneously possess excellent mechanical properties, skin self-adhesion, and outstanding conductivity, we utilize TA molecules to provide dynamic non-covalent bonds within the system. The zwitterionic polymer SBMA facilitates the dissociation of H$^+$ in the system, creating ion migration channels. PEI serves as a macromolecular crosslinker, forming intermolecular non-covalent bonds with TA, SBMA, and AAc to establish a physical crosslinking network. The chemical structures of SBMA, AAc, TA, PEI, and the preparation process of the SATP hydrogels are shown in Fig. 1a. The SATP hydrogel was synthesized *via* a one-pot method using free radical polymerization under UV irradiation. Through the synergistic effects of these components, including hydrogen bonding and electrostatic interaction, the SATP hydrogel achieves concurrent high strength, self-healing capability, and adhesive performance. This makes our SATP hydrogels promising as a wearable strain sensor for stable, real-time monitoring of human movement (Fig. 1b). And these multiple dynamic interactions in the network play two important roles in our hydrogel systems: providing sufficient non-covalent cross-linked sites achieve

gelation without the need for conventional chemical cross-linking, the porous network structure in SATP hydrogel was formed (Fig. S1); providing hydrogels with multiple interfacial sites for superior self-healing and excellent adhesion. Furthermore, Fourier-transform infrared spectroscopy (FT-IR) was performed to confirm the formation mechanism of SATP hydrogel, as shown in Fig. S2, the peak at 3442 cm^{-1} corresponded to the overlap of the N–H and O–H stretching vibrations in PEI, TA and AA.[31] The stretching vibration of C=O in SBMA and AA was observed at 1720 cm^{-1}.[32] At the same time, the bending vibration peak of the amine group (–NH$_2$ or –NH) peaks in PEI at 1572 cm^{-1} shifted to 1542 cm^{-1}, indicating that PEI, AAc, and SBMA were cross-linked by hydrogen bonding interaction. The symmetric stretching vibration peak (S=O) and asymmetric stretching vibration peak shifted to 1035 cm^{-1} and 1159 cm^{-1}, respectively, due to the formation of electrostatic interactions between SBMA molecules as well as hydrogen bonds with phenolic hydroxyl and amino groups.[33]

Mechanical properties

The formation of SATP hydrogels relies on diverse dynamic interactions between their components, including hydrogen bonds and electrostatic interactions. These dynamic interactions not only enhance the overall performance of the SATP hydrogels but also impart exceptional tensile properties. As
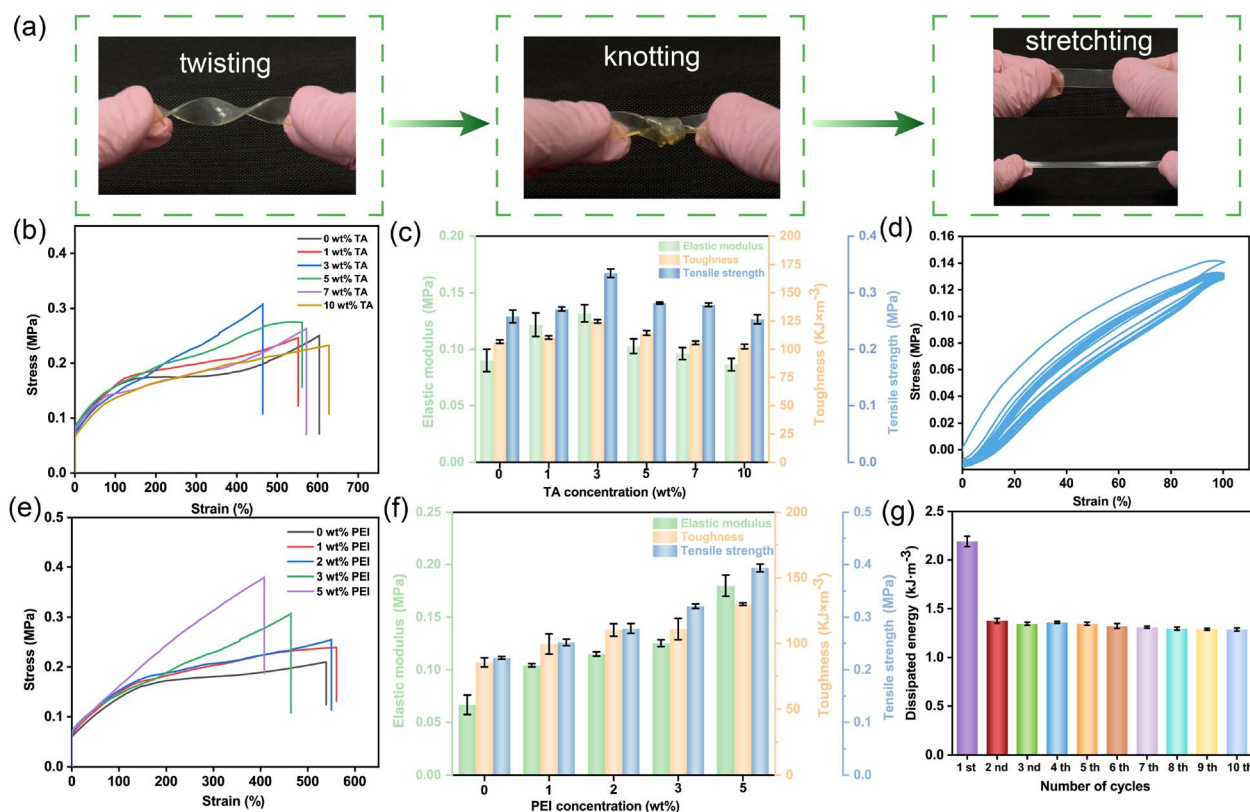

Fig. 2 Mechanical properties of SATP hydrogels. (a) Photographs of stretching, twisting, knotting and puncture resistance. (b) Tensile stress–strain curves and (c) the corresponding elastic modulus and toughness of SATP hydrogels with different TA content. (d) 10 cycles of tensile loading–unloading curves of SATP hydrogel at 100% strain. (e) Tensile stress–strain curves and (f) the corresponding elastic modulus and toughness of SATP hydrogels with different PEI concentration. (g) Dissipated energy of 10 tensile loading unloading cycle of SATP hydrogel at 100% strain.

28154 | *J. Mater. Chem. A*, 2025, **13**, 28152–28159

This journal is © The Royal Society of Chemistry 2025

shown in Fig. 2a, the SATP hydrogel exhibits sufficient flexibility to withstand stretching, knotting, and twisting. Meanwhile, it demonstrates remarkable puncture resistance. To gain deeper insights into the mechanical properties of the SATP hydrogels, the effects of TA and PEI content on the mechanical performance of the hydrogels were investigated, as illustrated in Fig. 2b and c. The tensile fracture strength of the hydrogel initially increases and then decreases along with increasing TA content from 0 wt% to 10 wt%. When the content of TA is 3 wt%, the mechanical properties are the best and the fracture stress reaches 0.31 MPa. Similar trends are observed for the elastic modulus and fracture toughness, which is attributed to the formation of additional physical crosslinking networks resulting from increasing of TA content. The internal dynamic reversible cross-linking interaction can effectively dissipate energy when hydrogels undergo deformation,[34] therefore, further improving its mechanical strength. However, when the TA content exceeds an optimal threshold, the tensile performance declines due to excessive physical crosslinking. This over-crosslinking softens the hydrogel and compromises its

mechanical properties. Consequently, a TA concentration of 3 wt% was selected for subsequent investigations.

Furthermore, as the PEI content increases, the tensile strength, elastic modulus, and toughness of the hydrogel continuously and significantly improve (Fig. 2e and f). This enhancement is attributed to PEI acting as a macromolecular crosslinker, forming additional hydrogen bonds with AAc, TA, SBMA, and itself, resulting in a denser network. This structural change is further confirmed by the SEM images (Fig. S1), thereby substantially boosting the mechanical properties of the SATP hydrogel. However, considering the interfacial characteristics and self-healing capability of the SATP hydrogel, excessive PEI consumes excessive binding sites, reducing both the self-healing efficiency and interfacial adhesion. Based on comprehensive testing, SATP hydrogels with 3 wt% TA and 3 wt% PEI were selected as the optimal formulation for subsequent studies. Furthermore, the long-term stability and anti-fatigue performance of the SATP hydrogel are prerequisites for its application in flexible sensors. Fig. 2d presents the cyclic tensile loading–unloading curves under 100% strain. Due to residual
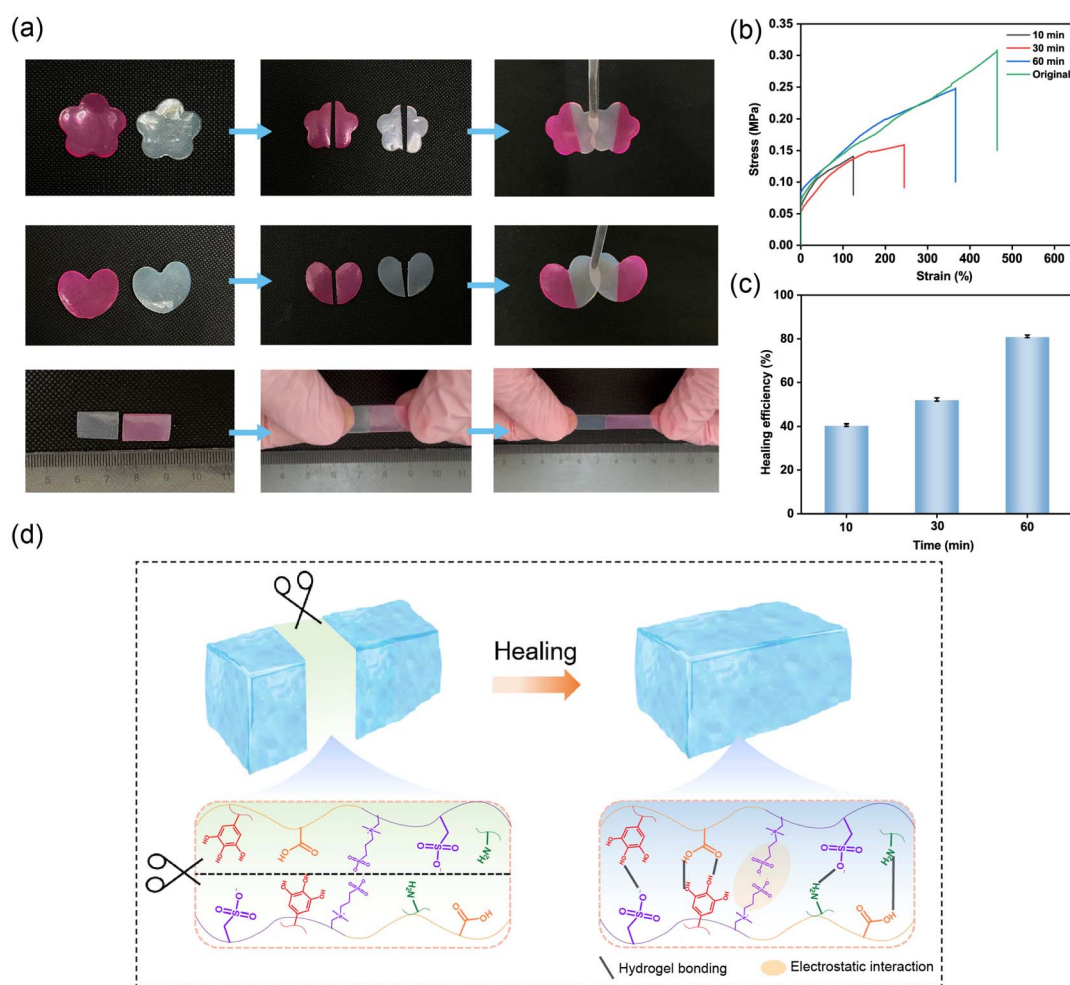

Fig. 3 (a) Optical images of two cut SATP hydrogels that heal after contact and when being deformed. (b) Typical stress−strain curves of the SATP hydrogel with different healing times. (c) Corresponding healing efficiency of the SATP hydrogel at different times. (d) Schematic illustration of dynamic reversible cross-links of the hydrogels.

This journal is © The Royal Society of Chemistry 2025

J. Mater. Chem. A, 2025, **13**, 28152–28159 | **28155**

strain, the cyclic curves exhibit pronounced hysteresis, yet the 10-cycle profiles maintain favorable energy dissipation.[35] After 10 cycles of loading–unloading at 100% strain, the tensile strength and dissipated energy of the material remain at 0.13 MPa and 1.3 kJ m^{-3}, respectively (Fig. 2g). During the loading–unloading process, the continuous breakage and reformation of hydrogen bonds and electrostatic interactions contribute to the stable mechanical performance of the SATP hydrogel.

Self-healing property

The self-healing property is essential for hydrogels to ensure long-term use in wearable devices. For SATP hydrogel, its self-healing capability originates from the abundant dynamic hydrogen bonds and electrostatic interactions within the cross-linked network. To evaluate the self-healing behavior, the SATP hydrogel sample was cut into two pieces with different shapes, as shown in Fig. 3a, and immediately brought into physical contact at room temperature. The hydrogel autonomously healed into an intact structure without additional external stimulation. The healed SATP hydrogel could still withstand mechanical deformation, such as stretching, demonstrating its robust self-healing ability to restore original mechanical properties. To visually investigate the self-healing performance, the conductive SATP hydrogel was connected in series with an LED bulb in a circuit. As illustrated in Fig. S3, the self-healed hydrogel successfully illuminated the LED bulb, with no significant change in brightness compared to the pristine state, thus confirming its excellent electrical self-healing capability. The properties of self-healing SATP hydrogels can also be quantitatively determined by measuring and recording the continuous changes of the cutting–healing cycle of the current. Even after multiple damages, SATP hydrogel can still restore its initial current time in a short period of time (Fig. S4). The self-healing efficiency, reflecting the hydrogel's restorative capacity, was also examined by comparing the mechanical strength of the healed hydrogel with the original sample (Fig. 3b). The SATP hydrogel exhibited time-dependent self-healing efficiency, recovering 80% of its original mechanical strength after 1 h of incubation (Fig. 3c). This outstanding self-healing behavior can be further understood at the molecular interaction level. Briefly, when the SATP hydrogel is severed, dynamic interactions such as hydrogen bonds and electrostatic forces are disrupted at the fracture interface. Upon contact between the two separated interfaces, these dynamic interactions rapidly regenerate, enabling network recovery at the wound site (Fig. 3d). The remarkable self-healing ability allows the hydrogel to promptly repair cracks and retain its intrinsic mechanical performance, thereby ensuring strong adaptability and higher reliability in complex real-world working environments.

Adhesive property

Reliable self-adhesion is a critical feature for wearable hydrogel sensors, distinguishing them from strain sensors that require additional adhesives.[31] This property ensures accurate electrical signal transmission by eliminating interfacial gaps between the

substrate and the hydrogel during sensing tests. Owing to the abundant –OH groups in TA and the charged characteristics of SBMA, the SATP hydrogel exhibits excellent adhesion, enabling tight attachment to diverse substrates, including wood, metal, glass, ceramics, and porcine skin (Fig. 4a). This superior adhesion arises from non-covalent interactions (hydrophobic interactions, hydrogen bonds, electrostatic interactions, and coordination bonds) formed between the SATP hydrogel and substrates. The adhesion strength of the hydrogel to different substrates was quantitatively evaluated via lap shear tests. As shown in Fig. 4b and c, the adhesion strength to wood, Fe, TA, glass, ceramics, and porcine skin were 11.8 kPa, 30.9 kPa, 38.4 kPa, 54.7 kPa, 62.8 kPa, and 122.1 kPa, respectively, surpassing those of previously reported hydrogels (Fig. 4d).[36–45] Notably, the SATP hydrogel exhibited the highest adhesion strength to porcine skin due to the formation of abundant hydrogen bonds between the –OH and –NH$_2$ on the skin surface and the SATP hydrogel.

To further investigate the adhesive performance, compressive adhesion tests were conducted. As illustrated in Fig. S5, the adhesion strength on various substrates gradually increased as the preloading force rose from 1 N to 3 N. This enhancement in adhesion strength is attributed to improved contact and increased interfacial area between the SATP hydrogel and substrates under higher loads. Additionally, repeatable and durable adhesion is crucial for practical applications. After 10 adhesion cycles (Fig. 4e), the adhesion strength of the hydrogel to porcine skin decreased from 123.7 kPa to 84.5 kPa,
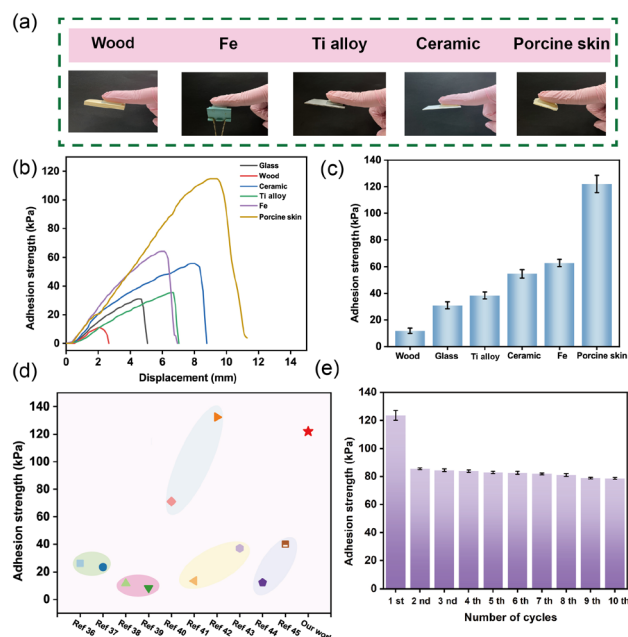

Fig. 4 (a) Photographs of SATP hydrogel adhering to various substrates. (b and c) The lap adhesion strength curves and corresponding statistics of SATP hydrogels on different substrates. (d) Comparison of the adhesion force of hydrogels with that reported in other literatures. (e) Ten cycles adhesion cycles under the continuous adhesion of SATP hydrogel on pig skin.

28156 | J. Mater. Chem. A, 2025, 13, 28152–28159

This journal is © The Royal Society of Chemistry 2025

demonstrating its durability and reusability. The slight reduction in adhesion strength may result from dust accumulation on the substrate surface during repeated tests. The stable and exceptional adhesion properties of the hydrogel ensure that deformations caused by human motion can be precisely converted into electrical signals, highlighting its reliability for wearable sensing applications.

Electrical property of the SATP hydrogel sensor

The ionic conductivity of hydrogels serves as a decisive characteristic for skin sensor applications. The interconnected porous structure of SATP hydrogel provides channels for ion migration, endowing the hydrogel with satisfactory conductive properties. Initially, the conductive SATP hydrogel was assembled into a complete circuit (Fig. S6). Upon stretching the hydrogel, the narrowed conductive pathways impeded ion transfer, resulting in increased hydrogel resistance and reduced LED bulb brightness.[46] These results demonstrated the hydrogel's significant electrical responsiveness to tensile strain. To

quantitatively investigate the relationship between electrical conductivity and strain, the resistance variation under applied strain was recorded using a universal tensile machine coupled with a digital source meter. As shown in Fig. 5a, $\Delta R/R_0$ progressively increased with tensile strain, indicating stable strain response across a wide strain range. The gauge factor (GF), a critical parameter for evaluating strain sensor sensitivity, was calculated from the slope of the $\Delta R/R_0$-strain curve.[47] Linear fitting revealed three distinct GF regions: 0.66 in the 0–100% strain range, 0.96 in the 100–200% range, and 1.27 in the 200–300% range. These results demonstrate desirable strain sensitivity over a broad deformation rang. Notably, the relative resistance change exhibited continuous and stable peak signals under repeated 50–250% strain cycles (Fig. 5b). Furthermore, the SATP hydrogel sensor maintained stable electrical signals through 50 stretching–releasing cycles, showcasing exceptional long-term stability and durability for flexible strain sensing applications (Fig. S7). Capitalizing on skin-like elasticity, desirable strain sensitivity, robust adhesion, self-healing capability, and environmental stability, the SATP hydrogel was
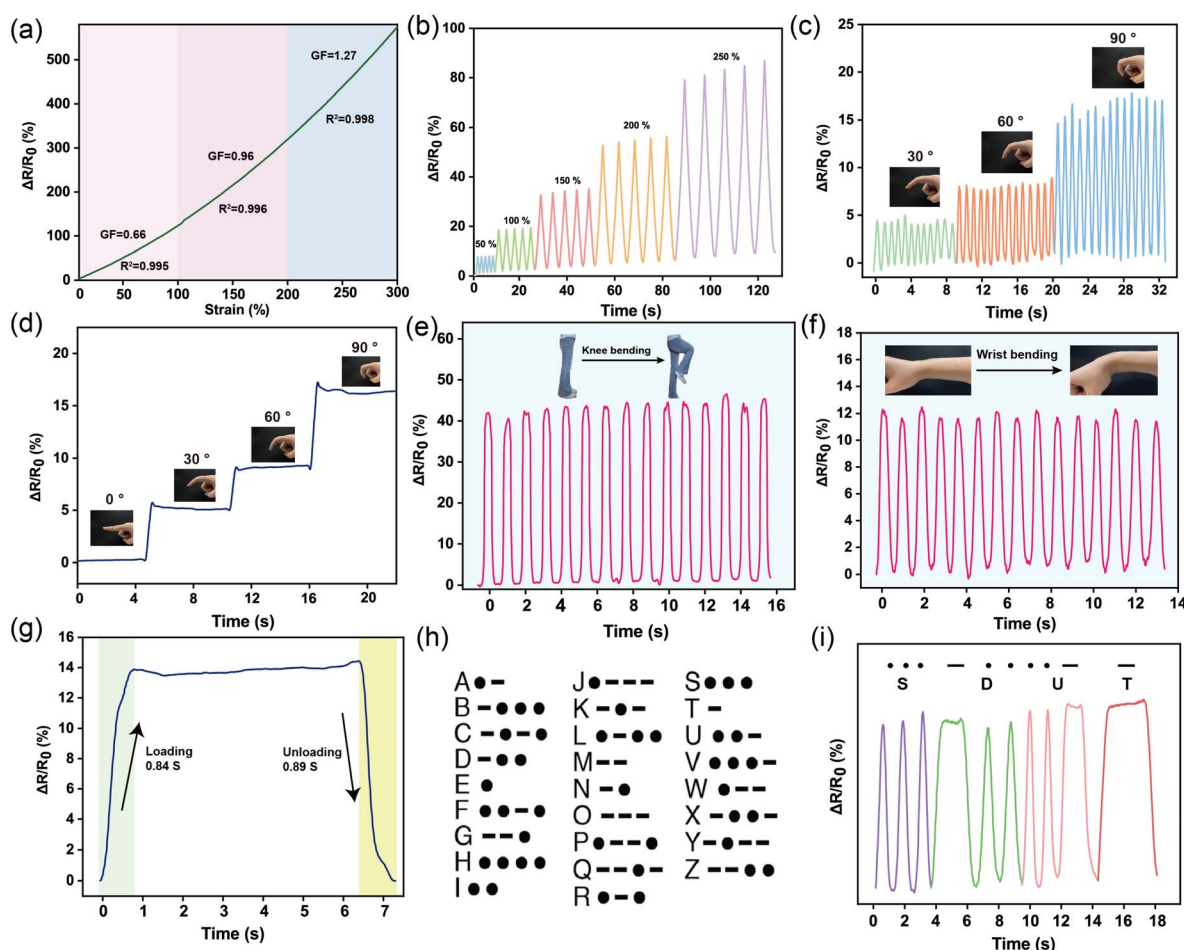

Fig. 5 (a) The relative resistance change ($\Delta R/R_0$) and the corresponding GF with continuous tensile strain from 0% to 300%. (b) $\Delta R/R_0$ changes under a stretching−releasing process at large strain (50%, 100%, 150%, 200%, 250%). (c) Signals of $\Delta R/R_0$ changes at different bending angles of finger joints. (d) The ladder $\Delta R/R_0$ changes for finger bending at different angles (0°, 30°, 60°, 90°). Signals of $\Delta R/R_0$ changes for monitoring different human movement, including knee bending (e) and wrist bending (f). (g) Response time under the instant strains. (h) The related symbols of the international Morse code alphabet. (i) Encrypting and transmitting of messages ("SDUT") by bending a finger regularly.

integrated into flexible wearable sensors for real-time human motion monitoring. During joint flexion (finger, knee, wrist, ankle), hydrogel stretching induced increased resistance. Fig. 5c and d illustrate $\Delta R/R_0$ variations during repeated finger bending at different angles (30°, 60°, 90°). The relative resistance peaks directly correlated with bending angles, returning to baseline upon finger extension, confirming the sensor's capacity to discriminate complex motions with angular precision. Consistent and reproducible electrical outputs were maintained throughout repetitive bending cycles. Similar resistance response patterns were observed for knee, wrist, and ankle movements (Fig. 5e, f, and S8), where joint flexion-induced stretching narrowed ionic channels and increased resistance. Beyond detecting large joint deformations, the sensor successfully captured subtle facial expressions like frowning (Fig. S9). The SATP hydrogel exhibited rapid response characteristics with 0.84 s response time and 0.89 s recovery time under strain (Fig. 5g), enabling precise real-time monitoring of human activities.

For information encryption applications, Morse code implementation was demonstrated through defined finger movements: rapid bending ("·") and sustained bending ("-") corresponded to sharp and flat resistance peaks, respectively. As exemplified in Fig. 5h and i, the characters "SDUT" were successfully encoded through programmed finger motions, while emergency "SOS" signals were reliably transmitted (Fig. S10). These comprehensive results underscore the significant potential of adhesive self-healing SATP hydrogels in practical wearable sensing devices for sophisticated human-machine interaction and information encryption systems.

Conclusions

A double-network SATP hydrogel with exceptional mechanical properties, favorable conductivity, robust adhesion, and rapid self-healing behavior was successfully fabricated *via* a facile one-pot method. The hydrogel achieved 80% self-healing efficiency within 1 h and exhibited high adhesive strength toward diverse substrates, particularly porcine skin (approximately 122.1 kPa). The outstanding performance of the SATP hydrogel originates from abundant dynamic hydrogen bonds at both intermolecular and intramolecular levels and electrostatic interactions. The assembled SATP hydrogel strain sensor demonstrated precise detection of strain stimuli (0–300%) with acceptable sensitivity (GF = 1.27), rapid response time (0.84 s), and signal stability. Notably, when attached to the human body, the SATP hydrogel sensor accurately captured subtle motions (*e.g.*, frowning) and large-scale limb movements (*e.g.*, finger, wrist, and knee flexion), enabling real-time monitoring of human activities. Furthermore, information encryption and transmission were achieved through finger-bending speed modulation. Overall, the proposed strain sensor exhibits satisfactory mechanical properties, adhesion performance, and conductivity, providing a promising design strategy for wearable sensors with robust self-healing capabilities and intimate adhesion.

Ethics statement

We ensure that all data relating to human motion sensing was performed in accordance with The Code of Ethics of the World Medical Association (Declaration of Helsinki). Our manuscript was in line with the Recommendations for the Conduct, Reporting, Editing and Publication of Scholarly Work in Medical Journals. This study has been approved by the ethics committee of Shandong University of Technology. Informed consent was obtained from all individual participants involved in the study prior to the commencement of any experimental procedures.

Author contributions

Yali Li: writing – original draft, investigation. Hui Liu: writing – review & editing, methodology, funding acquisition. Ruiyao Ma: software, data curation. Qiang Liu: funding acquisition. Shuanhong Ma: writing – review & editing, funding acquisition. Ning Han: writing – review & editing. Ling-Bao Xing: writing – review & editing, formal analysis, conceptualization.

Conflicts of interest

There are no conflicts to declare.

Data availability

All the data supporting this article have been included in the main text and the SI.

SEM morphology, FT-IR spectra, conductivity and self-healing performance, compressive adhesion strength, real-time relative resistance changes, sensing performance, coding application. See DOI: https://doi.org/10.1039/d5ta04564a.

Acknowledgements

Notes and references

1 C. Wang, T. He, H. Zhou, Z. Zhang and C. Lee, *Bioelectron. Med.*, 2023, **9**, 17–18.

2 W.-Y. Guo and M.-G. Ma, *J. Mater. Chem. A*, 2024, **12**, 9371–9399.

3 Z.-H. Yang, J. Yin, L. Xin, Y. Li, Y. Huang, R. Yuan and Y. Zhuo, *Chin. Chem. Lett.*, 2024, **35**, 109558.

4 B. Wang, W. Zhang, J. Sun, C. Lai, S. Ge, H. Guo, Y. Liu and D. Zhang, *J. Mater. Chem. A*, 2023, **11**, 8656–8669.

5 X. Nie, Y. Xie, X. Ding, L. Dai, F. Gao, W. Song, X. Li, P. Liu, Z. Tan and H. Shi, *Carbohydr. Polym.*, 2024, **334**, 122068.

6 H. Ding, J. Liu, X. Shen and H. Li, *Polymer*, 2023, **15**, 4001–4002.

28158 | *J. Mater. Chem. A*, 2025, **13**, 28152–28159

This journal is © The Royal Society of Chemistry 2025

7 Y. Liu, L. Wang, Y. Mi, S. Zhao, S. Qi, M. Sun, B. Peng, Q. Xu, Y. Niu and Y. Zhou, *J. Mater. Chem. C*, 2022, **10**, 13351–13371.

8 C. Zhao, Y. Wang, G. Tang, J. Ru, Z. Zhu, B. Li, C. F. Guo, L. Li and D. Zhu, *Adv. Funct. Mater.*, 2022, **32**, 2110417.

9 Z. Wang, H. Wei, Y. Huang, Y. Wei and J. Chen, *Soc. Rev.*, 2023, **52**, 2992–3034.

10 G. Chen, J. Huang, J. Gu, S. Peng, X. Xiang, K. Chen, X. Yang, L. Guan, X. Jiang and L. Hou, *J. Mater. Chem. A*, 2020, **8**, 6776–6784.

11 R. Zhu, Z. Zheng, D. Zhu and X. Wang, *J. Colloid Interface Sci.*, 2025, **677**, 687–696.

12 J. Lu, J. Gu, O. Hu, Y. Fu, D. Ye, X. Zhang, Y. Zheng, L. Hou, H. Liu and X. Jiang, *J. Mater. Chem. C*, 2021, **9**, 18406–18420.

13 A. Fuhrmann, R. Göstl, R. Wendt, J. Kötteritzsch, M. D. Hager, U. S. Schubert, K. Brademann-Jock, A. F. Thünemann, U. Nöchel and M. Behl, *Nat. Commun.*, 2016, **7**, 13623–13624.

14 K. Su, D. Deng, X. Wu, Y. Song, Y. Sun, X. Wang, Z. Zhang, J. Li, Z. Yan and X. Shang, *Chem. Eng. J.*, 2024, **479**, 147646.

15 K. Yang, J. Yang, R. Chen, Q. Dong and Y. Zhou, *ACS Appl. Mater. Interfaces*, 2024, **16**, 37569–37580.

16 L. Dai, Y. Geng, X. Ding, Z. Zhang, C. Lai, D. Zhang, C. Xia and Y. Lai, *Carbohydr. Polym.*, 2025, **10**, 123869.

17 G. Wang, Y. Liu, B. Zu, D. Lei, Y. Guo, M. Wang and X. Dou, *Chem. Eng. J.*, 2023, **455**, 140493.

18 H. Liu, X. Hu, W. Li, M. Zhu, J. Tian, L. Li, B. Luo, C. Zhou and L. Lu, *Chem. Eng. J.*, 2023, **452**, 139368.

19 J. Zhao, R. Chen, D. Cheng, X. Yang, H. Zhang, J. Zheng and R. Hu, *Adv. Funct. Mater.*, 2025, **35**, 2415530.

20 M. Wu, L. Han, B. Yan and H. Zeng, *Supramol. Mater.*, 2023, **2**, 100045.

21 Z. Li, J. Lu, T. Ji, Y. Xue, L. Zhao, K. Zhao, B. Jia, B. Wang, J. Wang and S. Zhang, *Adv. Mater.*, 2024, **36**, 2306350.

22 J. Wang, P. Du, Y.-I. Hsu and H. Uyama, *Chem. Eng. J.*, 2024, **480**, 148324.

23 J. Gu, J. Huang, G. Chen, L. Hou, J. Zhang, X. Zhang, X. Yang, L. Guan, X. Jiang and H. Liu, *ACS Appl. Mater. Interfaces*, 2020, **12**, 40815–40827.

24 J. Mo, Y. Dai, C. Zhang, Y. Zhou, W. Li, Y. Song, C. Wu and Z. Wang, *Mater. Horiz.*, 2021, **8**, 3409–3416.

25 X. Wang, Y. Wang, S. Bi, Y. Wang, X. Chen, L. Qiu and J. Sun, *Adv. Funct. Mater.*, 2014, **24**, 403–411.

26 F. Luo, T. L. Sun, T. Nakajima, T. Kurokawa, Y. Zhao, K. Sato, A. B. Ihsan, X. Li, H. Guo and J. P. Gong, *Adv. Mater.*, 2015, **27**, 2722–2727.

27 F. Zhao, E. Repo, Y. Song, D. Yin, S. B. Hammouda, L. Chen, S. Kalliola, J. Tang, K. C. Tam and M. Sillanpää, *Green Chem.*, 2017, **19**, 4816–4828.

28 J. Casper, S. H. Schenk, E. Parhizkar, P. Detampel, A. Dehshahri and J. Huwyler, *J. Controlled Release*, 2023, **362**, 667–691.

29 M. Gultekinoglu, Y. T. Sarisozen, C. Erdogdu, M. Sagiroglu, E. A. Aksoy, Y. J. Oh, P. Hinterdorfer and K. Ulubayram, *Acta Biomater.*, 2015, **21**, 44–54.

30 Z. Chen, Z. Lv, Y. Sun, Z. Chi and G. Qing, *J. Mater. Chem. B*, 2020, **8**, 2951–2973.

31 Z. Wang, H. Zhou, D. Liu, X. Chen, D. Wang, S. Dai, F. Chen and B. B. Xu, *Adv. Funct. Mater.*, 2022, **32**, 2201396.

32 C. Zhu, L. Zhang, A. Zou, W. Wang, J. Zhang and A. Zhang, *Chem. Eng. J.*, 2023, **475**, 146161.

33 P.-F. Ren, H.-C. Yang, H.-Q. Liang, X.-L. Xu, L.-S. Wan and Z.-K. Xu, *Langmuir*, 2015, **31**, 5851–5858.

34 C. Xu, J. Huang, Z. Guo and W. Liu, *Adv. Funct. Mater.*, 2025, **35**, 2413334.

35 Y. Zhou, L. Wang, Y. Liu, X. Luo, Y. He, Y. Niu and Q. Xu, *Chem. Eng. J.*, 2024, **484**, 149632.

36 L. Wu, S. Deng, J. Lai, L. Wang, G. Yan, C. Zhao, D. Xiang, H. Li, B. Wang and Z. Li, *Colloids Surf., A*, 2024, **688**, 133505.

37 Y. Wang, K. Zhong, Y. Mu, J. Xiang, T. Yao, K. Zhao, T. Gu and P. Jia, *Polymer*, 2025, **323**, 128210.

38 W. Zhang, P.-L. Wang, X.-X. Ji, L.-Z. Huang, D.-Q. Cao, J. Li and M.-G. Ma, *Composites, Part A*, 2024, **177**, 107957.

39 X. Xie, Y. Lei, Y. Li, M. Zhang, J. Sun, M.-Q. Zhu and J. Wang, *J. Colloid Interface Sci.*, 2023, **637**, 20–32.

40 X. Zhang, F. Li, S. Liang and Y. Bai, *Chem. Eng. J.*, 2024, **495**, 153385.

41 C. Wei, Y. Wang, Y. Liang, J. Wu, F. Li, Q. Luo, Y. Lu, C. Liu, R. Zhang and Z. Lu, *J. Mater. Chem. A*, 2024, **12**, 10392–10402.

42 Z. Ge, Z. Wang and C. Luo, *Int. J. Biol. Macromol.*, 2024, **266**, 131215.

43 G. Chen, O. Hu, J. Lu, J. Gu, K. Chen, J. Huang, L. Hou and X. Jiang, *Chem. Eng. J.*, 2021, **425**, 131505.

44 O. Hu, J. Lu, S. Weng, L. Hou, X. Zhang and X. Jiang, *Polymer*, 2022, **254**, 125109.

45 K. Wu, Y. Cui, Y. Song, Z. Ma, J. Wang, J. Li, T. Fei and T. Zhang, *Adv. Funct. Mater.*, 2023, **33**, 2300239.

46 S. Wang, X. Huang, H. Sun, F. Wang, B. Lei, W. Wang, Q. Wang, Y. Yang, J. Shao and X. Dong, *Chem. Eng. J.*, 2023, **478**, 147321.

47 H. Cai, D. Zhang, H. Zhang, M. Tang, Z. Xu, H. Xia, K. Li and J. Wang, *Chem. Eng. J.*, 2023, **472**, 144849.

This journal is © The Royal Society of Chemistry 2025

J. Mater. Chem. A, 2025, **13**, 28152–28159 | **28159**